Cerebral Cortex, May 2020;30: 3370–3380

doi: 10.1093/cercor/bhz315
Advance Access Publication Date: 20 February 2020
Original Article

ORIGINAL ARTICLE

Abundant Self-Amplifying Intermediate Progenitors in the Subventricular Zone of the Chinese Tree Shrew Neocortex

Chonghai Yin[1,2], Xin Zhou[2], Yong-Gang Yao[3,4,5], Wei Wang[2], Qian Wu[6,7] and Xiaoqun Wang[2,5,8]

[1]School of Life Science, University of Science and Technology of China, Hefei 230026, China, [2]State Key Laboratory of Brain and Cognitive Science, CAS Center for Excellence in Brain Science and Intelligence Technology, Institute of Brain-Intelligence Technology (Shanghai), Institute of Biophysics, Chinese Academy of Sciences, Beijing, 100101, China, [3]Kunming Primate Research Center of the Chinese Academy of Sciences, Kunming Institute of Zoology, Chinese Academy of Sciences, Kunming 650223, China, [4]CAS Center for Excellence in Brain Science and Intelligence Technology, Chinese Academy of Sciences, Shanghai 200031, China, [5]University of Chinese Academy of Sciences, Beijing 100049, China, [6]State Key Laboratory of Cognitive Neuroscience and Learning, Beijing Normal University, Beijing 100875, China, [7]IDG/McGovern Institute for Brain Research, Beijing Normal University, Beijing, 100875, China, and [8]Beijing Institute for Brain Disorders, Beijing 100069, China

Address correspondence to Wei Wang. Email: wangwei@ibp.ac.cn; Qian Wu. Email: qianwu@bnu.edu.cn; Xiaoqun Wang. Email: xiaoqunwang@ibp.ac.cn.

Abstract

During evolution, neural progenitor cells in the subventricular zone (SVZ) have fundamental functions, ranging from brain volume expansion to the generation of a six-layered neocortex. In lissencephalic animal models, such as rodents, the majority of neural progenitors in the SVZ are intermediate progenitor cells (IPCs). Most IPCs in rodents undergo neurogenic division, and only a small portion of them divide a very limited number of times to generate a few neurons. Meanwhile, in gyrencephalic animals, such as primates, IPCs are able to self-renew for up to five successive divisions. However, abundant IPCs with successive proliferative capacity have not been directly observed in nonprimate species. In this study, we examined the development of neural progenitors in the Chinese tree shrew (*Tupaia belangeri chinensis*), a lissencephalic animal with closer affinity than rodents to primates. We identified an expansion of the SVZ and the presence of outer radial glial (oRG) cells in the neocortex. We also found that IPCs have the capacity to self-amplify multiple times and therefore serve as major proliferative progenitors. To our knowledge, our study provides the first direct evidence of abundant IPCs with proliferative potential in a nonprimate species, further supporting the key role of IPCs in brain expansion.

Key words: Chinese tree shrew, neural progenitors, intermediate progenitor, self-amplifying proliferation

Introduction

The neocortex is evolutionarily the most recent part of the cerebral cortex and appears to be a distinguishing feature of mammals. It is the seat of advanced cognitive capability, sensory perception, and emotional manipulation. During evolution, the volume and the neuronal population of the neocortex expanded considerably (Rakic 2009). How the expansion of the neocortex is

precisely regulated in different species is therefore a fundamental and fascinating question. In the last two decades, remarkable progress has been achieved in the field of neural development (Gotz and Huttner 2005; Rakic 2009; Lui et al. 2011; Taverna et al. 2014; Lein et al. 2017). There is ample evidence that the diversity and complexity of neural progenitor cells (NPCs) are critical for brain volume expansion during evolution (Taverna et al. 2014; Florio et al. 2017; Goffinet 2017; Llinares-Benadero and Borrell 2019). Broadly, neural progenitors in the mammalian neocortex can be classified into two major types based on their position during mitosis: apical progenitors (APs) and basal progenitors (BPs); APs and BPs are assembled into two germinal zones which was named by the Boulder Committee, the ventricular zone (VZ) and the subventricular zone (SVZ), respectively (Rakic 2003; Bystron et al. 2008). APs, consisting of neuroepithelial cells (NE) at the early embryonic stage and radial glial cells at the neurogenic stage, are primary progenitors with considerable proliferation capacity and can give rise to apical progenitors, basal progenitors and postmitotic neurons via symmetric and/or asymmetric proliferation (Gotz and Huttner 2005; Kriegstein and Alvarez-Buylla 2009; Rakic 2009).

BPs populate the SVZ and display diverse proliferative capacities. The formation of the SVZ is the hallmark of the generation of the six-layered neocortex, and the emergence of BPs is considered a key governor of neocortical expansion (Miyata et al. 2004; Noctor et al. 2004; Kriegstein et al. 2006; Rakic 2009; Florio and Huttner 2014; Goffinet 2017). However, the thickness of the SVZ varies greatly in different species. In primates, the SVZ expands substantially at the peak of neurogenesis and becomes subdivided into the inner SVZ (iSVZ) and outer SVZ (oSVZ) (Smart et al. 2002; Kriegstein and Alvarez-Buylla 2009; Lui et al. 2011; Betizeau et al. 2013; Molnar et al. 2014; Dehay et al. 2015; Lein et al. 2017). Similar to the thickness of SVZ, the cellular diversity and proliferative capacity of BPs also differ greatly in different species. In rodents, the major type of BP is the intermediate progenitor cell (IPC); IPCs express Tbr2 and generally divide once or a very limited number of times to generate a few neurons (Haubensak et al. 2004; Miyata et al. 2004; Noctor et al. 2004; Vasistha et al. 2015; Mihalas and Hevner 2018).

Studies in humans, macaques and ferrets have led to the identification of a new subtype of BPs, named oRG cells, in the SVZ. These progenitors maintain long basal processes, share the expression of several genes (e.g., Pax6 and Sox2, but not Tbr2) with RGs, and have the capacity to proliferate multiple times (Fietz et al. 2010; Hansen et al. 2010; Reillo et al. 2011). In primates, the relative abundance of oRG cells at the peak of neurogenesis accounts for more than 75% of BPs (Betizeau et al. 2013; Dehay et al. 2015). In contrast, in rodents, oRG cells are rare (less than 10% of BPs) (Shitamukai et al. 2011; Wang et al. 2011; Nelson et al. 2012). To date, the existence of the oSVZ and oRG cells has been demonstrated in several species, both lissencephalic and gyrencephalic ones (Garcia-Moreno et al. 2012; Kelava et al. 2012). It has been proposed that the origin of the oSVZ and oRG cells is ancestral to the emergence of primates and that the oSVZ and oRG cells are not exclusive to the gyrencephalic brain but instead represent an evolutionarily conserved compartmentalization (Hevner and Haydar 2012; LaMonica et al. 2013; Molnar et al. 2014; Dehay et al. 2015; Goffinet 2017).

In addition to oRG cells, IPCs are also considered to have been instrumental in the evolution of neocortical thickness and surface expansion. Human and macaque IPCs in the SVZ can undergo up to five rounds of self-renewal before producing neurons (Hansen et al. 2010; Betizeau et al. 2013; Florio and Huttner 2014), suggesting that cortical expansion may be further explained by an increased number of IPCs. Note that the ability of IPCs to divide repeatedly is documented in primates but is much less robust in other mammals (Haubensak et al. 2004; Noctor et al. 2004; Hevner and Haydar 2012; Vasistha et al. 2015). This suggests that the proliferative capacity of IPCs might have been enhanced during evolution along the primate lineage.

To address this question, we used the Chinese tree shrew (*Tupaia belangeri chinensis*), which has a closer affinity than rodents to primates (Fan et al. 2013; Lin et al. 2014), to detect the development and progenitor characteristics of the neocortex. The Chinese Tree shrew is a squirrel-like animal with a gestation period of 40–45 days. Additionally, tree shrews have a higher brain to body mass ratio than any other mammals, including humans (Wong and Kaas 2009). Therefore, it has been suggested as a good model to study brain development and evolution.

In this study, we reported a cytoarchitectonic analysis of the Chinese tree shrew and showed that its SVZ expands remarkably at midgestation, especially between E35 and E40. Contrary to rodents, the Chinese tree shrew exhibits an obvious oSVZ and abundant oRG cells as well as IPCs residing in both the iSVZ and the oSVZ. Time-lapse recording and EdU/BrdU dual-pulse tracing results indicated that IPCs in the Chinese tree shrew have the ability to proliferate successively and serve as one of the major types of basal progenitors. To our knowledge, our study provides the first direct evidence of abundant self-amplifying IPCs in a nonprimate species, further supporting the key role of IPCs in brain expansion.

Materials and Methods

Animals

Chinese tree shrews were obtained from the Kunming Institute of Zoology, Chinese Academy of Sciences. Animal housing and all experimental procedures were in compliance with the guidelines of the Institutional Animal Care and Use Committee of the Institute of Biophysics and Kunming Institute of Zoology, Chinese Academy of Sciences. To obtain embryos, each male Chinese tree shrew was housed with one female. All cages were under surveillance with video cameras, and copulation behaviors were analyzed based on recorded images as described before (Yan et al. 2016). Successful copulation was considered embryonic day 0 (E0). Pregnancy was confirmed based on body weight gain of the females after 1 week. Then, timed-pregnant animals were subjected to various treatments.

Immunohistochemistry

The pregnant females were anesthetized with isoflurane and sacrificed. Following intracardiac perfusion with cold PBS (pH 7.4) and 4% PFA in PBS (pH 7.4), the brains of the embryos were removed and fixed in PFA overnight at 4 °C. The fixed brains were cryopreserved in 20% and 30% sucrose in PBS sequentially at 4 °C and embedded in optimal cutting temperature compound. Sections (10 μm) were prepared using a cryostat (Leica CM3050 S). For immunohistochemistry, antigen retrieval was performed by incubating sections in 0.01 M sodium citrate (pH 6.0) for 20 min at 90–95 °C, and then primary antibody incubation was performed overnight at 4 °C. Incubation with secondary antibodies was performed for 1–2 h at room temperature. The primary antibodies were rabbit anti-Tbr2 (1:200, Abcam, ab23345), mouse anti-Ki67 (1:500, BD

Biosciences, 556 003), rabbit anti-phospho-Histone 3 (1:500, Cell Signaling, 9701 s), rat anti-BrdU (1:200, Serotec, MCA2060GA), rabbit anti-Pax6 (1:200, Covance, PRB-278P), goat anti-Sox2 (1:200, Santa Cruz, sc17319), and mouse anti-phospho-Vimentin (1:200, Abcam, ab22651). Secondary antibodies conjugated to Alexa 488, 594 or 647 were used at a 1:500 dilution based on the primary antibodies used. Nuclei were counter-stained with DAPI. Images were acquired with an Olympus FV1000 confocal microscope and edited with Fluoview (Olympus) and Photoshop (Adobe Systems).

The images were acquired with a Leica stereotype microscope and edited with Photoshop.

EdU and BrdU Dual-Pulse Labeling

To monitor the proliferation of Tbr2^{+} IPCs, EdU (50 mg/kg body weight) was administered interperitoneally to timed-pregnant animals (at E25 and E30). After 24 h, BrdU (Sigma, 50 mg/kg body weight) was introduced. The animals were sacrificed after 2 h, and the embryos were dissected and fixed in 4% PFA. BrdU immunostaining and EdU reactions were carried out as described.

In-Utero Viral Infection

The uterine horns of anesthetized timed-pregnant dams were exposed through midline laparotomy. GFP-expressing AAV (adeno-GFP, 1 µl) with Fast Green (0.1 mg/ml, Sigma) was injected into the lateral ventricle of embryos with a beveled, calibrated glass micropipette (Drummond Scientific). Throughout the surgical procedures, the uteri were constantly bathed with warm phosphate-buffered saline (PBS, pH 7.4). After injection, the uterine horns were placed back in the abdomen, which was surgically closed.

Slice Culture and Time-Lapse Imaging

Brains were sectioned with a vibrating microtome as previously described (Hansen et al. 2010; Wang et al. 2011). Briefly, the brains were embedded in 3% low-melting-temperature agarose in ice-chilled artificial cerebrospinal fluid (ACSF) and vibratome-sectioned at 200 µm in ice-chilled ACSF. The slices were transferred to slice culture inserts (Millipore) with medium in culture plates. The cultures were incubated at 37 °C with a constant 5% CO_2 supply. For time-lapse imaging, brain slices were cultured in medium containing 66% neurobasal medium, 25% HBSS, 5% FBS, 1% N-2 medium, 1% penicillin/streptomycin/glutamine (Invitrogen), and 0.66% D-(+)-glucose (Sigma). CMV–GFP adenovirus (2×10^3 c.f.u.) was microinjected focally in the paraventricular regions to achieve sparse labeling. Time-lapse images were acquired using an inverted laser scanning microscope (Olympus Fluoview FV1000) equipped with a ×10 air objective lens (zoom 2) every 15–30 min for approximately 72 h. Maximum intensity projections of the collected stacks were compiled into movies and analyzed using ImageJ software.

Cell Cleavage Plane Analysis

Mitotic cells were identified by phospho-H3 immunofluorescence. The cleavage plane angles were calculated by determining the angle between cytokinesis and the ventricular surface with ImageJ software.

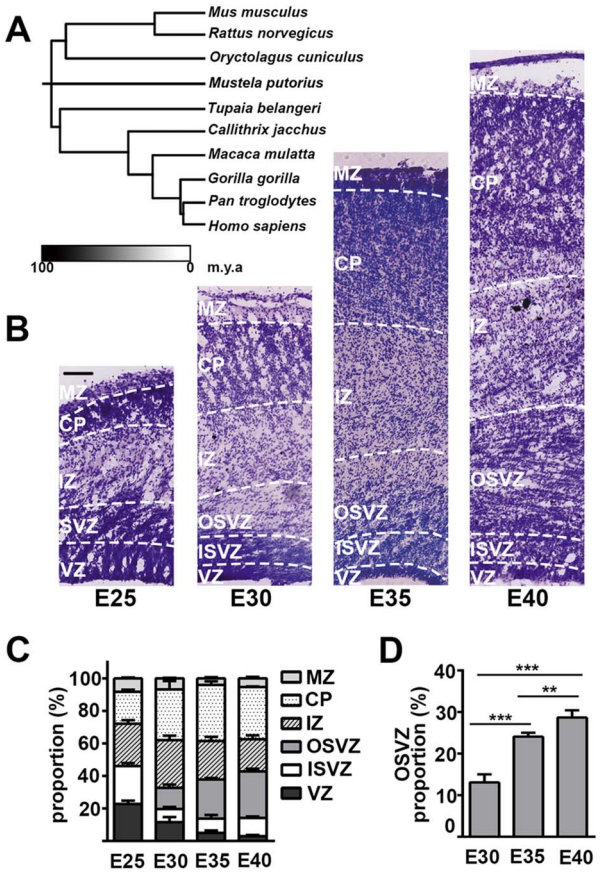

Figure 1. Analysis of neocortex compartmentalization of the Chinese tree shrew. (*A*) Evolutionary relationships between the tree shrew and mammalian species. A schematic phylogenetic tree showing that the tree shrew, compared with mouse and ferret, has a closer affinity to primates. y.m.a., million years ago. (modified from Fan et al. 2013). (*B*) Nissl staining of coronal sections of the Chinese tree shrew forebrain at various stages of embryonic development. VZ, ventricular zone; SVZ, subventricular zone; iSVZ, inner subventricular zone; oSVZ, outer subventricular zone; IZ, intermediate zone; CP, cortical plate. MZ, marginal zone. Scale bar: 50 µm. (*C*) The oSVZ developed at E30 in the developing Chinese tree shrew forebrain. Neocortical compartment proportions were calculated and compared at different developmental stages. The data are shown as the mean ± s.d. of three individual experiments. (*D*) The oSVZ expanded rapidly during the development of the Chinese tree shrew forebrain from E30 to E40. The data are shown as the mean ± s.d. of three individual experiments. Unpaired two-tailed Student's *t*-test was used, $^{*}P < 0.05$, $^{**}P < 0.01$, $^{***}P < 0.001$, and $^{****}P < 0.0001$.

Statistics

All experiments used at least three animals, and all other experiments were carried out at least in triplicate, as indicated in the figure legends. The error bars are the s.d. Statistical analysis was calculated by the unpaired two-tailed Student's *t*-tests and the multiple comparison test after ANOVA using GraphPad prism software, and the significance levels were $^{*}P < 0.05$, $^{**}P < 0.01$, $^{***}P < 0.001$, and $^{****}P < 0.0001$.

Result

The SVZ, Especially the oSVZ, is Expanded Remarkably in the Neocortex of the Chinese Tree Shrew

The adult Chinese tree shrew brain has a smooth surface with a rhinal fissure separating the neocortex from the olfactory

cortex (Fig. S1A,B). As the Chinese tree shrew is phylogenetically closer than rodents to primates (Fig. 1A), we decided to study the compartmentation of its brain with a focus on the neocortex. Nissl staining was used to define the cytoarchitecture of the neocortex at different embryonic stages (E25, E30, E35, and E40).

The thickness of the cerebral wall increased gradually from E25 to E40 (Fig. 1B). The cortices of the Chinese tree shrew at E25 comprised two germinal layers, a cell-dense VZ and an adjacent thin SVZ located above the VZ, as previously documented in mice (Bystron et al. 2008). A relatively highly cell-dense cortical plate (CP) that was separated from the germinal layers by a cell-sparse intermediate zone (IZ) and bordered externally by the marginal zone was also distinguishable at this stage (Fig. 1B). At this stage, the cortical cytoarchitecture resembled that of the E13 mouse brain.

From E30, the thickness of the cerebral wall increased gradually, and there was a dramatic expansion of the SVZ, which is the most significant difference between mouse and Chinese tree shrew cortices (Fig. 1B). Quantification showed that the thickness of the SVZ increased by almost a factor of three from E30 to E40 (Fig. 1C,D). In parallel, the thickness of the VZ decreased from ~25% (E25) to ~5% (E40). To verify that the expanded region corresponded to a proliferative germinal zone and not the intermediate zone, we performed Ki67 immunohistochemistry and counterstaining with DAPI to label proliferating cells (Fig. S1C). The results showed that, at E25, Ki67$^+$ cells were concentrated in the VZ, and there were a few outside the VZ, indicating the emergence of the SVZ, in accordance with the data obtained by Nissl staining. After E30, Ki67$^+$ cells expanded basally. A discrete Ki67$^+$ population was readily detected outside of the SVZ, indicating the formation of the oSVZ as described previously (Reillo et al. 2011; Garcia-Moreno et al. 2012). At E40, the number of Ki67$^+$ cells peaked (Fig. S1C). Thus, we found that the SVZ, especially the oSVZ, expanded prominently in the neocortex of the Chinese tree shrew.

Basal Progenitors are Abundant in the SVZ of the Chinese Tree Shrew Neocortex at Later Stages

Based on the cytoarchitecture illustrated by Nissl staining and the proliferation profiled by Ki67, we inferred that three germinal zones were present in the neocortex of the Chinese tree shrew. To examine the distribution and relative abundance of different neural progenitor cells, we first used Sox2 and Tbr2 to estimate the number of RG/oRG cells and IPCs at distinct developmental stages.

At E25, Sox2$^+$ cells were densely packed in the VZ, and there were some in the SVZ; Tbr2$^+$ cells bordered the basal boundary of the SVZ (Fig. 2A). At E30, the number of Sox2$^+$ cells in the VZ was decreased, but not dramatically; the number in the SVZ was increased. The number of Tbr2$^+$ cells was also increased in the SVZ (Fig. 2B), and the iSVZ and the oSVZ were observed at this stage. At later stages (E35 and E40), the thickness of the oSVZ increased substantially, and this increase was accompanied by a sharp decline in the thickness of the VZ. Meanwhile, a massive increase in the number of Sox2$^+$ and Tbr2$^+$ cells in the oSVZ, resembling what has been reported in primates and carnivores (Fietz et al. 2010; Hansen et al. 2010; Reillo et al. 2011; Betizeau et al. 2013), was also observed, indicating the high abundance of oRG and IPCs (Fig. 2C–F). Interestingly, we also noticed a decrease in the number of Tbr2$^+$ cells in the iSVZ at E35 and E40 (Fig. 2F), which was in line with the decrease in the number of Sox2$^+$ cells in the iSVZ at these two stages (Fig. 2E). In contrast, a burst of Tbr2$^+$ cells was observed in the oSVZ, and this was accompanied by an overwhelming increase in the number of Sox2$^+$ cells in the oSVZ (Fig. 2E,F). This suggested that these Tbr2$^+$ cells might originate from Sox2$^+$ cells in the oSVZ. In addition to Sox2$^+$ or Tbr2$^+$ cells in the SVZ, we also observed some cells coexpressing Sox2 and Tbr2, as reported in humans, macaques, and ferrets. However, the proportion of all cells that were Sox2$^+$Tbr2$^+$ at distinct stages was 6–17%, which was similar to the proportion in humans but far less than the proportions in macaques and ferrets (Hansen et al. 2010; Reillo et al. 2011; Betizeau et al. 2013).

To verify that the Sox2$^+$ cells in the oSVZ were oRG cells, time-lapse imaging and immunostaining were used. First, we introduced adeno-GFP into the lateral ventricle of the developing neocortices of E30 embryos by in-utero injection. We searched for GFP$^+$ cells with oRG morphology 2 days after infection and observed GFP$^+$ monopolar cells in the SVZ (Fig. 3 and Movie 1). Similar to oRG cells in the human fetal brain and mouse cortex, these GFP$^+$ monopolar cells each had a long basal process, did not make contact with the ventricles, and underwent mitotic somal translocation. After one cell cycle, one of the two siblings retained the basal process, indicating the nature and self-renewal/proliferative ability of oRG cells (Fig. 3 and Movie 1). Of note, we did not observe oRG-like cells with apical processes or with both apical and basal processes, two subtypes that can be readily detected in macaques (Betizeau et al. 2013).

We also used immunohistochemistry to examine whether cells with oRG-like morphology expressed the transcription factors Pax6 and Sox2, neural stem and progenitor cell markers that are expressed by human and mouse RG and oRG cells. We utilized phospho-Vimentin (p-Vim), a cytoplasmic marker of mitotic cells, to delineate their morphology.

At E25, 70–80% of the triple-positive cells (Sox2$^+$Pax6$^+$p-Vim$^+$), which were RG cells, were located in the VZ, and each harbored a long process that protruded to the basal pia. In addition to the triple-positive cells that harboring basal processes in the VZ, we also observed some dividing cells without basal processes at the most apical surface, which may have been apical intermediate progenitors (aIPs, indicated in Fig. 4A with asterisks) (Gal et al. 2006; Tyler and Haydar 2013). At E30, a surge in the number of oRG-like triple-positive cells in the SVZ was detected. We found that more than 70% of the triple-positive cells were located in the SVZ (both the iSVZ and the oSVZ), and 50% of triple-positive cells with basal processes in the SVZ were recorded (Fig. 4A,C). At E35 and E40, the size of the oSVZ increased as development progressed, indicating the continuous generation and proliferation of oRG cells (Fig. 4A,C). In parallel with the massive generation of neurons, the relative proportion of dividing cells decreased gradually (Fig. 4B, Fig. S1C).

Oblique Spindle Orientation of RG Cells Promoted the Production of oRG Cells

Next, we asked whether and how oRG cells were generated from RG cells. To address.

this, low-titer GFP-expressing adenovirus was administered into the ventricles of embryonic brains to visualize the division of neural progenitor cells. We found that, in the VZ, RG cells migrated interkinetically during the cell cycle, as has been observed in other species, suggesting a conserved mechanism (Gotz and Huttner 2005; Bystron et al. 2008). Briefly, RG cells that were attached to the ventricular surface with apical processes migrated apically from the abventricular zone and divided at the most apical surface (Fig. 5A and Movie 2). After division, one of

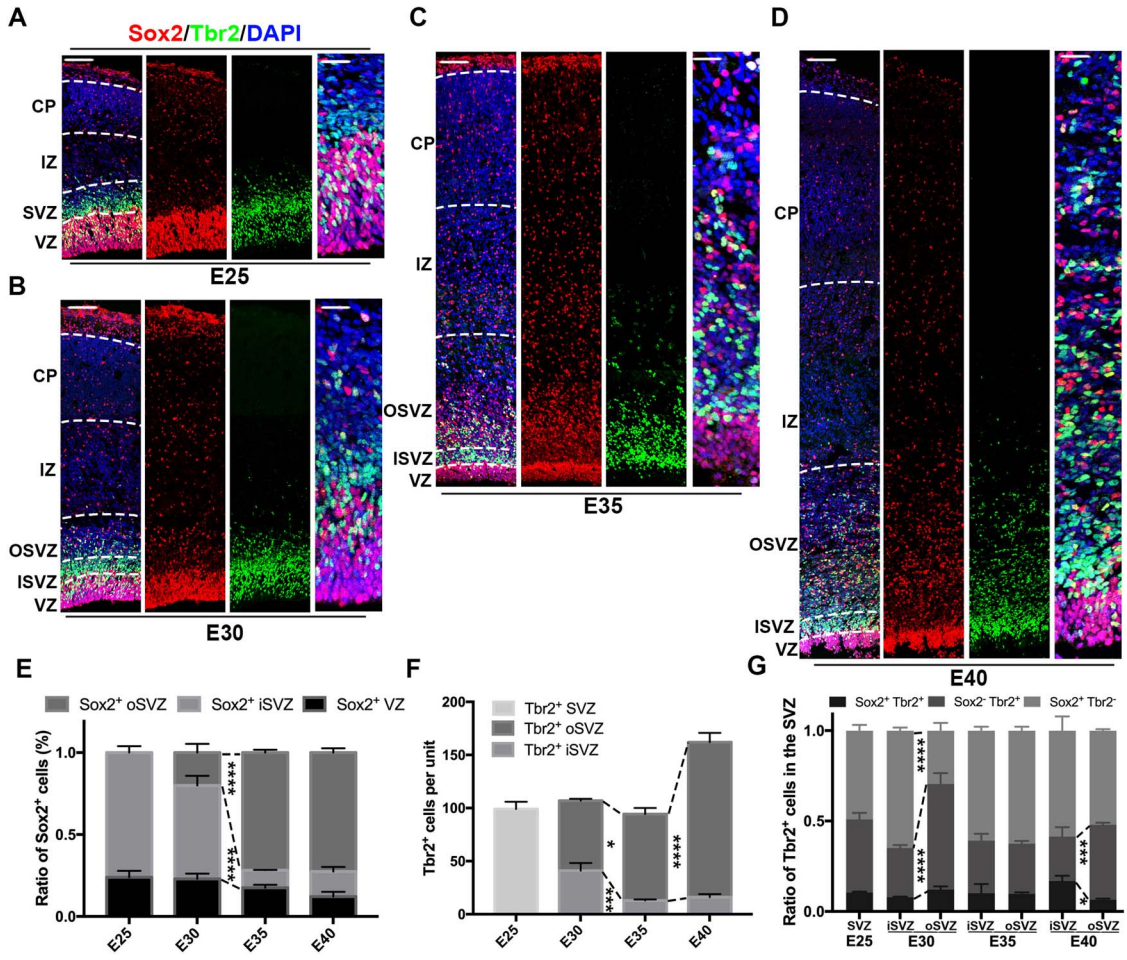

Figure 2. Distribution and relative abundance of neural progenitors in the neocortex of the Chinese tree shrew. (*A–D*) Images showing the distribution of $Sox2^+$ and $Tbr2^+$ cells in the neocortex at various stages of development in the Chinese tree shrew. $Sox2^+$ RG cells were dense in the VZ, and the thickness decreased from E25 to E40, while the number of $Sox2^+$ oRG cells gradually increased in the SVZ, both in the iSVZ and the oSVZ. $Tbr2^+$ IPCs expanded remarkably in the SVZ. Scale bar: 100 μm and 50 μm (zoomed images). (*E–G*) Quantification of $Sox2^+$ and $Tbr2^+$ cell distribution at different stages of development. The data are shown as the mean ± s.d. of three animals. (*E*) Quantification of $Sox2^+$ cell distribution in the VZ and the SVZ of the Chinese tree shrew. (*F*) The absolute number of $Tbr2^+$ cells in different compartments of the Chinese tree shrew neocortex. (*G*) The distribution and relative proportion of BPs in the SVZ of the Chinese tree shrew. The data are shown as the mean ± s.d. of three individual experiments at each stage. The multiple statistical analysis after ANOVA was shown in Supplementary File, $^*P < 0.05$, $^{**}P < 0.01$, $^{***}P < 0.001$, and $^{****}P < 0.0001$.

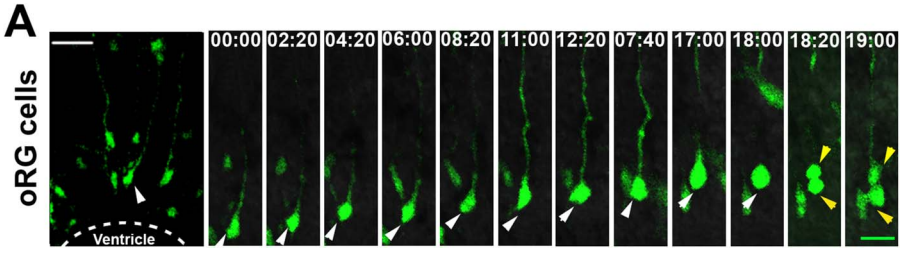

Figure 3. Morphology and cell-cycle parameters of oRG cells in the Chinese tree shrew. (*A*) Typical morphology and division patterns of oRG cells were recorded with time-lapse imaging after the introduction of adeno-GFP. The cell shown here was located in the oSVZ and had a long basal process that protruded to the pial surface and underwent mitotic somal translocation. White arrowhead: mother cell; yellow arrowhead: daughter cells after division. Scale bars: 50 (white) and 15 μm (yellow). Time:h:min. The experiments were carried out in triplicate, 15 time-lapse images were recorded.

the daughters inherited the basal process, and the other retained the apical process, indicating asymmetric cell fate; the cells that inherit the basal process may represent oRG cells (Fig. 5A and Movie 2).

We observed from the time-lapse recording that the division plane during the generation of oRG cells from RG cells was horizontal (Fig. 5A). To ascertain this, we measured the division plane angle relative to the apical surface or the VZ at different

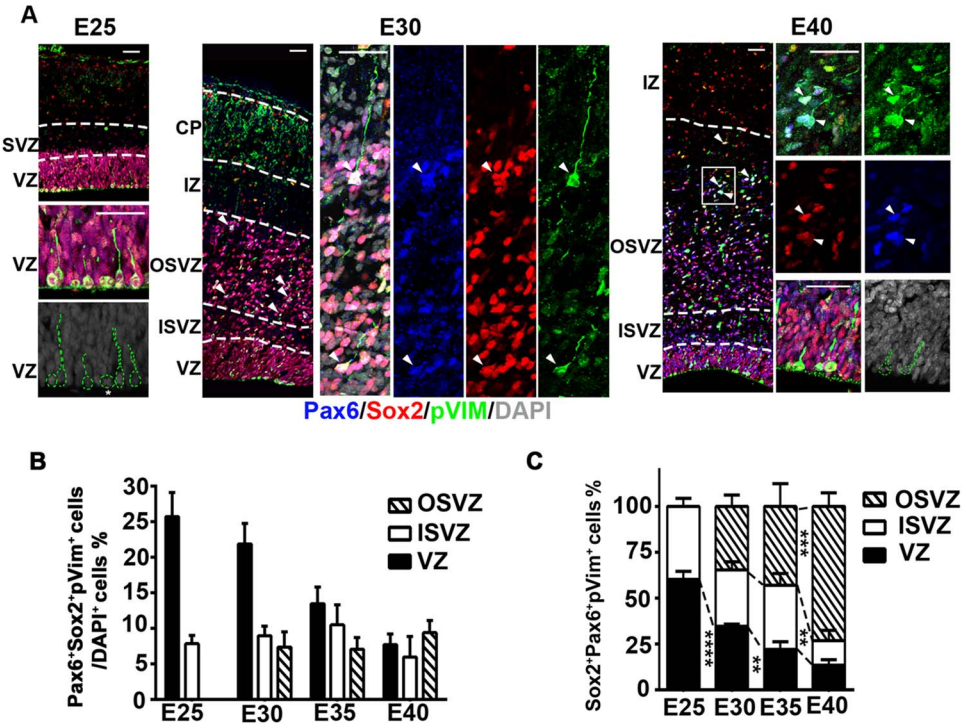

Figure 4. oRG cells were abundant in the developing neocortex of the Chinese tree shrew. (*A*) Sox2 and Pax6 expression at E25 was mostly confined to the VZ, but there were a few labeled cells in the SVZ. From E30 on, $Sox2^+$ and $Pax6^+$ cells occupied the area above the VZ, which was considered the OSVZ. Dividing RG cells were outlined by p-Vim staining at E25 and E40. oRG cells were identified as cells expressing Sox2, Pax6, and p-Vim with basal processes. oRG cells were present from E30 on. Arrowheads: oRG cells; asterisks: apical intermediate progenitors. Scale bar: 50 μm. (*B*) Quantitative analysis of $Sox2^+$, $Pax6^+$, and p-Vim^+ cells in different germinal zones at different stages of development. (*C*) The proportion of $Sox2^+$, $Pax6^+$, and p-Vim^+ cells in the VZ, iSVZ, and oSVZ at different stages of development. The data are shown as the mean ± s.d. of three individual experiments. For more detail, the multiple statistical analysis after ANOVA was shown in Supplementary File, $^*P < 0.05$, $^{**}P < 0.01$, $^{***}P < 0.001$, and $^{****}P < 0.0001$.

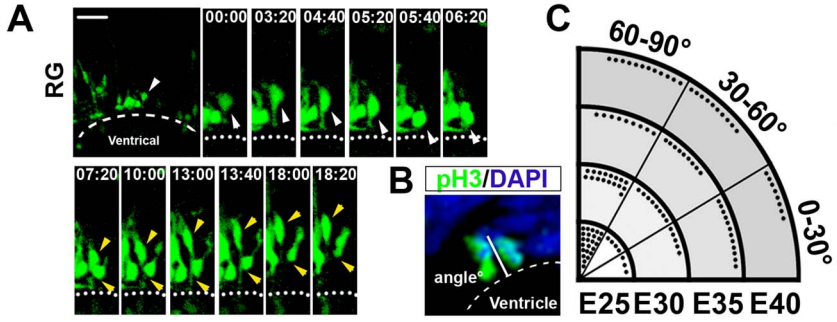

Figure 5. Morphology and cell-cycle parameters of RG cells in the Chinese tree shrew. (*A*) A representative RG cell was recorded. The RG cell migrated from the basal boundary of the VZ to the apical surface to divide and generated one cell that maintained the apical process and one that inherited the basal process via asymmetric division. White arrowhead: mother cell; yellow arrowhead: daughter cells after division. Scale bars: 50 and 15 μm. Time:h:min. Totally, 10 time-lapse images were recorded. (*B*) The cleavage angle was measured by staining for pH3, and DAPI was used to outline chromosomes at the VZ surface. (*C*) Quantitative analysis of cleavage angles of mitotic cells in the VZ of the Chinese tree shrew at E25, E30, E35, and E40. The majority of cells divided vertically at the early stage. More cells shifted to horizontal and oblique division from E30.

stages by immunohistochemistry for pH3, which labels separating chromosomes in M-phase (Fig. 5B). The results showed that, at E25, most of the dividing cells (~80%) underwent vertical division. However, from E30 on, the ratio of oblique or horizontal division increased to near 50% (Fig. 5C), in line with observations in human embryos (LaMonica et al. 2013).

Taken together, our data indicated that, in the neocortex of the Chinese tree shrew, abundant oRG cells were present in the SVZ at later stages. The mitotic division plane in RG cells shifted from vertical to nonvertical (oblique and horizontal) from E30, which may have increased the output of oRG cells.

IPCs Underwent Successive Divisions

In addition to the abundant occurrence of oRG cells in the SVZ at later stages, we also observed numerous $Tbr2^+$ (both $Sox2^+$ and $Sox2^-$) IPCs in the SVZ, especially in the oSVZ (Fig. 2). At E40, $Tbr2^+Sox2^-$ cells accounted for over 40% of the total neural

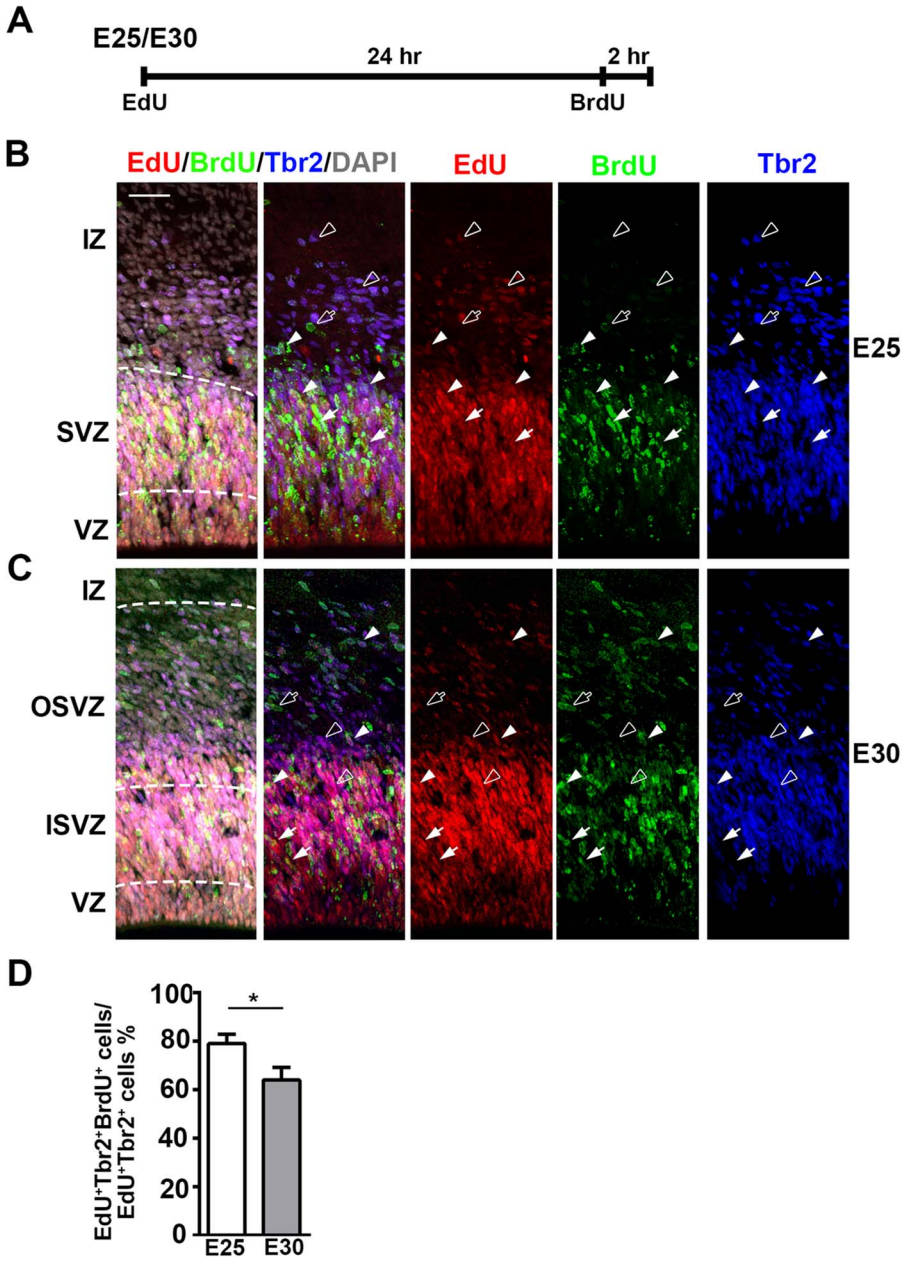

Figure 6. IPCs are highly proliferative in the Chinese tree shrew. (*A*) Proliferating cell labeling strategy. (*B*) EdU and BrdU dual-pulse labeling revealed a sustained strong proliferative ability of $Tbr2^+$ cells in the SVZ at E25 and E30. The major proliferating region was in the SVZ. Arrow: EdU^+BrdU^+ cells; open arrow: $BrdU^+$ cells; arrowhead: $EdU^+BrdU^+Tbr2^+$ cells; open arrowhead: EdU^+Tbr2^+ cells. Scale bars: 50 μm. (*C*) Quantification of the proportion of $EdU^+Tbr2^+BrdU^+$ cells relative to EdU^+Tbr2^+ cells at E25 and E30. The majority of proliferating IPCs entered the second cell cycle in 24 h. The data are shown as the mean ± s.d. of three individual experiments. Unpaired two-tailed student's *t*-test was used, $^*P < 0.05$.

progenitors in the oSVZ (Fig. 2G). The intermediate progenitor hypothesis emphasizes the fundamental function of IPCs in brain volume expansion (Kriegstein et al. 2006; Lui et al. 2011). In humans and macaques, the discovery of the successive proliferation of IPCs confirmed this hypothesis (Hansen et al. 2010; Betizeau et al. 2013; Florio and Huttner 2014; Dehay et al. 2015). As the Chinese tree shrew has a closer phylogenetic relationship than rodents or carnivores to primates, we wondered whether IPCs in the Chinese tree shrew have self-amplifying capacity.

To assess this, we performed dual-pulse labeling with EdU and BrdU at 24 h intervals (Fig. 6A). If a cell re-entered S-phase within 24 h following the administration of EdU, which is incorporated into DNA in S-phase, BrdU was incorporated into its DNA. We found that most $Tbr2^+$ cells were labeled with both EdU and BrdU (~80% at E25 and ~60% at E30, Fig. 6B–D), showing that $Tbr2^+$ cells underwent a second round of mitosis within 24 h.

To consolidate the conclusion, we performed time-lapse recording in cultured brain slices. After infecting cells with adeno-GFP, we observed that round-shaped cells in the oSVZ underwent at least two rounds of cell division in our recording time window. An example is shown in Fig. 7A. The cell in the oSVZ divided horizontally to generate two daughter cells. After

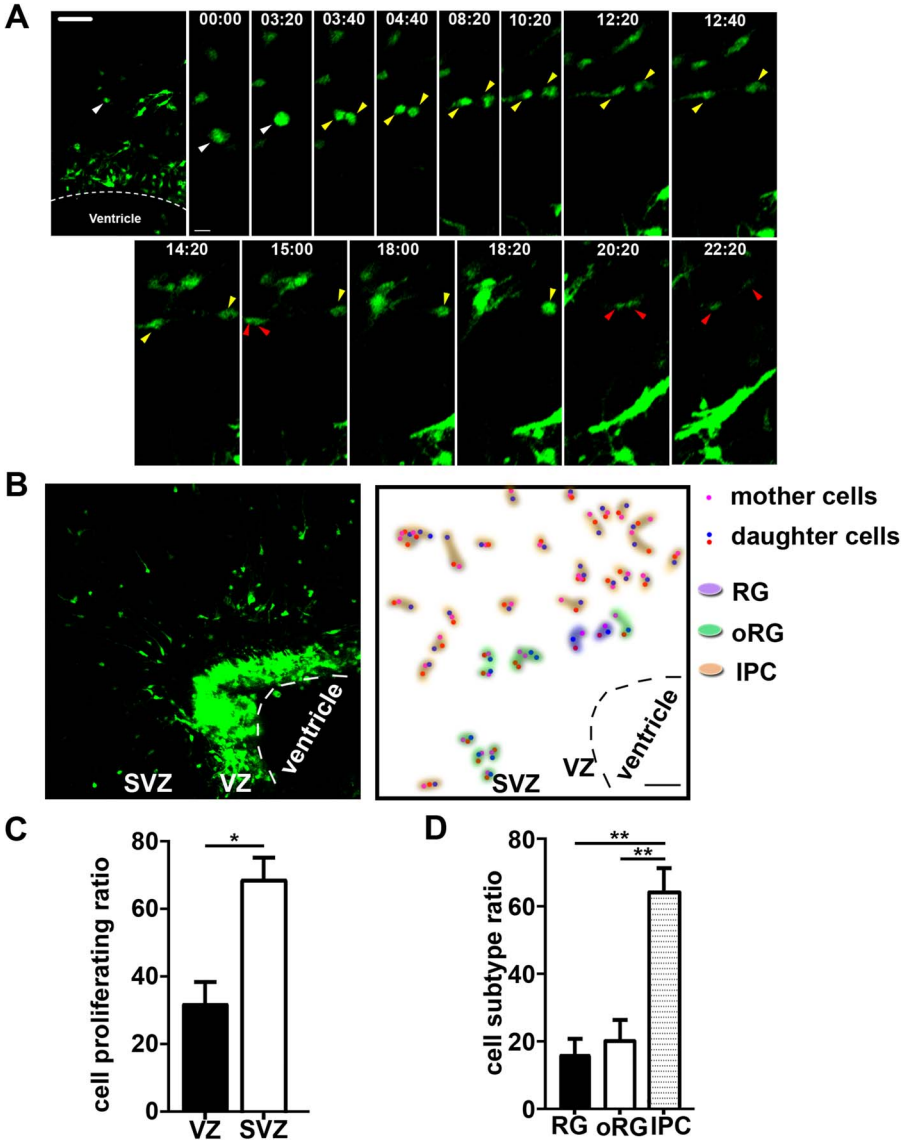

Figure 7. Successive IP divisions, as viewed by time-lapse imaging. (*A*) A representative example of an IPC cell in the SVZ dividing twice. White arrowhead: mother IPC cell; yellow arrowhead: daughter cells after the first division; red arrowhead: daughter cells from the second cell cycle. Scale bars: 50 and 15 μm. Time:h:min. (*B*) Progenitor cell divisions in the VZ and the SVZ at E30. The pink dots represent cells that are dividing; the red and blue dots are daughter cells generated by adjacent purple cells. Cells with processes that were located near the ventricle and divided in INM pattern were RG cells. Cells with basal fibers in the SVZ were oRG cells. Other cells that divided symmetrically were IPCs. The purple shadows, green shadows, and orange shadows illustrate the dividing area of RG cells, oRG cells and IPCs. (*C*) Quantification of the distribution of proliferating cells in the Chinese tree shrew cortex. The cells located in the SVZ were more active than those in the VZ. (*D*) The proportion of dividing progenitors in the VZ and the SVZ in the Chinese tree shrew. IPCs were the major proliferating cells in the VZ/SVZ. The data are shown as the mean ± s.d. of three individual experiments, 13 time-lapse images were recorded. Unpaired two-tailed Student's *t*-test was used, $^{*}P < 0.05$, $^{**}P < 0.01$.

12 h, one of the daughter cells divided once more, and the other daughter cell underwent mitosis 5 h later (Fig. 7A and Movie 3). Unlike oRG cells, these progenitors were round in morphology and lacked elongated basal processes, and all of them divided horizontally, indicating that they were indeed IPCs.

Using time-lapse imaging at E30, we quantified dividing cells and their lineages, as shown in Fig. 7B. We also inferred that cells located in the SVZ were more active than those in the VZ at E30 (Fig. 7C) because the SVZ started to expand around E30 (Figs 1B, 2B, S1C). IPCs are the major type of dividing progenitors at this stage (Fig. 7D), whereas in other species with an expanded SVZ, oRG cells are more preponderant (Fietz et al. 2010; Hansen et al. 2010; Reillo et al. 2011).

Taken together, the EdU and BrdU dual-pulse labeling data in combination with the time-lapse recording data, indicated that IPCs in the SVZ can undergo multiple proliferative divisions. In addition, our quantification showed that IPCs are the major BPs in the Chinese tree shrew cortex and presumably contribute to its development and expansion.

Discussion

In this study, we analyzed the subtypes, distribution, and proliferation characteristics of neural progenitors in the neocortex of the Chinese tree shrew (Fig. 8). We observed an expanded SVZ subdivided into the iSVZ and the oSVZ at E30 that became

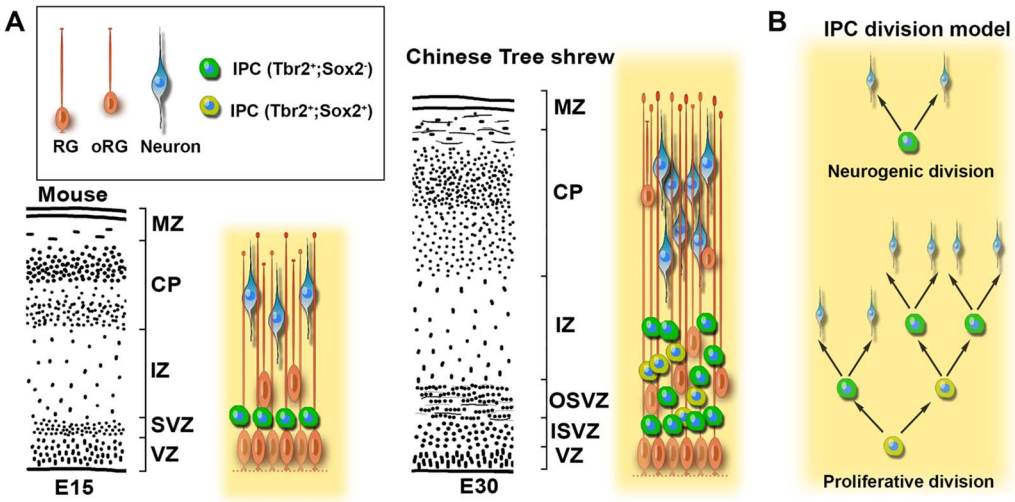

Figure 8. Schematic of neocortical architecture and a model of IP division in the mouse and Chinese tree shrew at midgestation. (A) The Chinese tree shrew neocortex at E30 consists of a cell-dense VZ and a large SVZ, which include the iSVZ and an oSVZ. The oSVZ has a filament-like structure compared with the mouse at E15. There are two types of $Tbr2^+$ IPCs that can be distinguished by the coexpression of Sox2 in the Chinese tree shrew. (B) Models of the neurogenic and proliferative division of IPCs. In mice, most IPCs undergo symmetric neurogenic division. In Chinese tree shrews and primates, abundant IPCs undergo successive proliferative division, which might be related to the expression of Sox2.

more evident at E35 and E40. Abundant BPs, including oRG cells and IPCs, were readily detected in the SVZ. IPCs were the major proliferating progenitors in the SVZ. By using a combination of dual-pulse labeling and time-lapse recording, we observed the abundant successive proliferation of IPCs in a nonprimate species, specifically in the neocortex of the Chinese tree shrew, for the first time.

The Proliferative Capacity of IPCs Might be Enhanced during Evolution

IPCs, which express Tbr2, have been proposed to have a key role in cortical expansion (Lui et al. 2011). During evolution from stem amniotes to mammals, the cerebral cortex probably evolved from a three-layered dorsal cortex to a six-layered neocortex, owing to the emergence of intermediate progenitors and the formation of the SVZ (Martinez-Cerdeno et al. 2006; Cheung et al. 2010). In rodents, most $Tbr2^+$ IPCs undergo neurogenic division with fewer (~7.5%) undergoing multiple rounds of cell division before generating neurons (Haubensak et al. 2004; Noctor et al. 2004; Mihalas and Hevner 2018). In humans and macaques, a large number of IPCs that undergo up to five rounds of division have been detected (Hansen et al. 2010; Betizeau et al. 2013). The intermediate progenitor model has proposed that the symmetric proliferative division of IPCs, compared with symmetric neurogenic division, can more rapidly expand the neuronal number. Studies of IPCs division in rodents and primates have given rise to the hypothesis that the proliferative capacity of IPCs might be increased during evolution to accelerate neuronal production. However, no direct evidence has been found in nonprimate animals.

Here, we observed that many IPCs can undergo multiple rounds of proliferative division in the Chinese tree shrew by using time-lapse recording and BrdU/EdU dual-pulse labeling. Our observations provided direct evidence that supports the intermediate progenitor hypothesis. However, how many rounds of division these IPCs can undergo is not clear due to technical restrictions. Moreover, the molecular mechanisms governing the proliferative versus neurogenic division of IPCs are still elusive. In our study, we observed that 6–16% of precursors coexpressed Tbr2 and Sox2 in the SVZ of the Chinese tree shrew. In mice, most SVZ cells express Pax6 or Tbr2 but not both (Englund et al. 2005; Wang et al. 2011). The proportion increases to up to 80% in the iSVZ and to 20–25% in the oSVZ of the macaque occipital cortex (Betizeau et al. 2013). Currently, it is still elusive whether there is any difference in the proliferative capacity between $Tbr2^+Sox2^-$ and $Tbr2^+Sox2^+$ IPCs. Betizeau and colleagues suggested that IPCs with sustained Sox2 and Pax6 expression have a greater proliferative capability (Betizeau et al. 2013; Dehay et al. 2015). Therefore, we believe that single-cell RNA seq analysis will provide more instructive information on the distinct features of $Tbr2^+$ subtypes ($Sox2^+$ and $Sox2^-$), and more elaborative experiments should be designed to verify them.

Occurrence of oRG Cells and the oSVZ is not Sufficient for Brain Folding

Since the seminal discovery of oRG cells in the oSVZ of gyrencephalic animals, their function and contribution to brain expansion and folding have been widely debated (Hevner and Haydar 2012; LaMonica et al. 2012; Dehay et al. 2015; Llinares-Benadero and Borrell 2019). To date, oSVZ and oRG cells have been discovered in different mammalian branches from rodents to primates, both in gyrencephalic and lissencephalic brains (Fietz et al. 2010; Hansen et al. 2010; Lui et al. 2011; Reillo et al. 2011; Shitamukai et al. 2011; Wang et al. 2011; Garcia-Moreno et al. 2012; Hevner and Haydar 2012; Kelava et al. 2012; Nelson et al. 2012; Betizeau et al. 2013; Sauerland et al. 2018). Additionally, neurogenesis is complete before gyrification begins. It seems that an expanded oSVZ and oRG cells are not sufficient for brain folding. Recent study in primate cerebrum indicates that oSVZ gliogenesis, rather than neurogenesis, correlates with rapid enlargement of the cerebrum and the formation of brain folding (Rash et al. 2019). However, there is no doubt that oRG

cells contribute to an increase in brain volume expansion. In humans, macaques, and ferrets, the percentage of oRG cells relative to all progenitors reaches ~50% (Fietz et al. 2010; Hansen et al. 2010; Reillo et al. 2011; Betizeau et al. 2013; Dehay et al. 2015), and oRG cells serve as the major progenitors for brain expansion. Here, we demonstrated the presence of oRG cells in another lissencephalic animal, the Chinese tree shrew. We observed an expanded oSVZ with abundant oRG cells (more than 50% relative to total BPs) in the neocortex, thus confirming the hypothesis that the division of the SVZ and the emergence of oRG cells are essential for the enlargement of neuronal outputs but not sufficient for brain folding, as addressed elsewhere (Garcia-Moreno et al. 2012; Hevner and Haydar 2012; Kelava et al. 2012; LaMonica et al. 2013; Goffinet 2017; Sauerland et al. 2018).

Distinct Features Exist between the Chinese and Northern Tree Shrews

Recently, Prof. Fietz and colleagues reported data on the presence, abundance, and distribution of bRG (oRG) cells and other distinct NPCs in the developing neocortex of the Northern tree shrew (*Tupaia belangeri*) (Romer et al. 2018). We found some differences between the Chinese and Northern tree shrews. First, in the Chinese tree shrew, nearly all of the oRG cells detected had basal processes, whereas in the Northern tree shrew, several subtypes of oRG cells with different morphologies, such as oRG-apical-P, oRG-both-P, and oRG-basal-P and bTG cells, were observed, as also documented in the macaque (Betizeau et al. 2013). Second, in the Northern tree shrew, the majority of $Tbr2^+$ IPCs in the SVZ also expressed Pax6 (~70%). In contrast, in the Chinese tree shrew, we observed that fewer than 20% of $Tbr2^+$ IPCs coexpressed Sox2, a marker equivalent to Pax6 in the neocortex (Hansen et al. 2010). These differences indicate that the Northern and Chinese tree shrews underwent specific evolutionary adaption after their phyletic divergence (Fan et al. 2013). Hence, it may prove interesting to compare both subspecies and decipher how environment, diet, and geography impact neural development.

Concluding Remarks

The expansion of brain volume relies heavily on the temporal and spatial modulation of different progenitors. During evolution, different species use different strategies for neocortical neurogenesis. Successive divisions of oRG cells may be an efficient way to generate a thick neocortex. Our study emphasizes the essential role of IPCs, especially self-amplifying IPCs, in neocortical development. Given its specific evolutionary relationship to the primate lineage, we propose that the Chinese tree shrew will prove a useful model for studying neural development and evolution, as also considered by others (Fan et al. 2013; Yao 2017; Romer et al. 2018).

Supplementary Material

Supplementary material is available at *Cerebral Cortex* online.

Funding

National Basic Research Program of China (2017YFA0103303, 2019YFA0110100 and 2017YFA0102601); Strategic Priority Research Program of the Chinese Academy of Sciences (XDA16020601 and XDB32010100); the National Natural Science Foundation of China (NSFC) (31671072, 31671073, 31771140, 81891001 and 91732301); the Grants of Beijing Brain Initiative of Beijing Municipal Science & Technology Commission (Z181100001518004); and the Grants of Shanghai Brain-Intelligence Project from STCSM (16JC1420500).

Notes

We thank the lab members of Wang lab for their discussions and comments on this study. We also thank Prof. Andre Goffinet for his professional suggestions and comments. *Conflict of Interest*: None declared.

References

Betizeau M, Cortay V, Patti D, Pfister S, Gautier E, Bellemin-Ménard A, Afanassieff M, Huissoud C, Douglas Rodney J, Kennedy H *et al*. 2013. Precursor diversity and complexity of lineage relationships in the outer subventricular zone of the primate. *Neuron*. 80:442–457.

Bystron I, Blakemore C, Rakic P. 2008. Development of the human cerebral cortex: boulder committee revisited. *Nat Rev Neurosci*. 9:110–122.

Cheung AFP, Kondo S, Abdel-Mannan O, Chodroff RA, Sirey TM, Bluy LE, Webber N, DeProto J, Karlen SJ, Krubitzer L *et al*. 2010. The subventricular zone is the developmental milestone of a 6-layered neocortex: comparisons in Metatherian and Eutherian mammals. *Cereb Cortex*. 20:1071–1081.

Dehay C, Kennedy H, Kosik KS. 2015. The outer subventricular zone and primate-specific cortical complexification. *Neuron*. 85:683–694.

Englund C, Fink A, Lau C, Pham D, Daza RA, Bulfone A, Kowalczyk T, Hevner RF. 2005. Pax6, Tbr2, and Tbr1 are expressed sequentially by radial glia, intermediate progenitor cells, and postmitotic neurons in developing neocortex. *J Neurosci*. 25:247–251.

Fan Y, Huang ZY, Cao CC, Chen CS, Chen YX, Fan DD, He J, Hou HL, Hu L, Hu XT *et al*. 2013. Genome of the Chinese tree shrew. *Nat Commun*. 4:1426. doi: 10.1038/ncomms2416

Fietz SA, Kelava I, Vogt J, Wilsch-Brauninger M, Stenzel D, Fish JL, Corbeil D, Riehn A, Distler W, Nitsch R *et al*. 2010. OSVZ progenitors of human and ferret neocortex are epithelial-like and expand by integrin signaling. *Nat Neurosci*. 13:690–699.

Florio M, Borrell V, Huttner WB. 2017. Human-specific genomic signatures of neocortical expansion. *Curr Opin Neurobiol*. 42:33–44.

Florio M, Huttner WB. 2014. Neural progenitors, neurogenesis and the evolution of the neocortex. *Development*. 141:2182–2194.

Gal JS, Morozov YM, Ayoub AE, Chatterjee M, Rakic P, Haydar TF. 2006. Molecular and morphological heterogeneity of neural precursors in the mouse neocortical proliferative zones. *J Neurosci*. 26:1045–1056.

Garcia-Moreno F, Vasistha NA, Trevia N, Bourne JA, Molnar Z. 2012. Compartmentalization of cerebral cortical germinal zones in a lissencephalic primate and gyrencephalic rodent. *Cereb Cortex*. 22:482–492.

Goffinet AM. 2017. The evolution of cortical development: the synapsid-diapsid divergence. *Development*. 144:4061–4077.

Gotz M, Huttner WB. 2005. The cell biology of neurogenesis. *Nat Rev Mol Cell Biol*. 6:777–788.

Hansen DV, Lui JH, Parker PRL, Kriegstein AR. 2010. Neurogenic radial glia in the outer subventricular zone of human neocortex. *Nature*. 464:554–561.

Haubensak W, Attardo A, Denk W, Huttner WB. 2004. Neurons arise in the basal neuroepithelium of the early mammalian telencephalon: a major site of neurogenesis. *Proc Natl Acad Sci U S A*. 101:3196–3201.

Hevner RF, Haydar TF. 2012. The (not necessarily) convoluted role of basal radial glia in cortical neurogenesis. *Cereb Cortex*. 22:465–468.

Kelava I, Reillo I, Murayama AY, Kalinka AT, Stenzel D, Tomancak P, Matsuzaki F, Lebrand C, Sasaki E, Schwamborn JC *et al*. 2012. Abundant occurrence of basal radial glia in the subventricular zone of embryonic neocortex of a lissencephalic primate, the common marmoset *Callithrix jacchus*. *Cereb Cortex*. 22:469–481.

Kriegstein A, Alvarez-Buylla A. 2009. The glial nature of embryonic and adult neural stem cells. *Annu Rev Neurosci*. 32:149–184.

Kriegstein A, Noctor S, Martínez-Cerdeño V. 2006. Patterns of neural stem and progenitor cell division may underlie evolutionary cortical expansion. *Nat Rev Neurosci*. 7: 883.

LaMonica BE, Lui JH, Hansen DV, Kriegstein AR. 2013. Mitotic spindle orientation predicts outer radial glial cell generation in human neocortex. *Nat Commun*. 4.

LaMonica BE, Lui JH, Wang X, Kriegstein AR. 2012. OSVZ progenitors in the human cortex: an updated perspective on neurodevelopmental disease. *Curr Opin Neurobiol*. 22: 747–753.

Lein ES, Belgard TG, Hawrylycz M, Molnar Z. 2017. Transcriptomic perspectives on neocortical structure, development, evolution, and disease. *Annu Rev Neurosci*. 40(40):629–652.

Lin J, Chen G, Gu L, Shen Y, Zheng M, Zheng W, Hu X, Zhang X, Qiu Y, Liu X *et al*. 2014. Phylogenetic affinity of tree shrews to Glires is attributed to fast evolution rate. *Mol Phylogenet Evol*. 71:193–200.

Llinares-Benadero C, Borrell V. 2019. Deconstructing cortical folding: genetic, cellular and mechanical determinants. *Nat Rev Neurosci*. 20:161–176.

Lui JH, Hansen David V, Kriegstein Arnold R. 2011. Development and evolution of the human neocortex. *Cell*. 146:18–36.

Martinez-Cerdeno V, Noctor SC, Kriegstein AR. 2006. The role of intermediate progenitor cells in the evolutionary expansion of the cerebral cortex. *Cereb Cortex*. 16(Suppl 1):i152–i161.

Mihalas AB, Hevner RF. 2018. Clonal analysis reveals laminar fate multipotency and daughter cell apoptosis of mouse cortical intermediate progenitors. *Development*. 145:dev164335.

Miyata T, Kawaguchi A, Saito K, Kawano M, Muto T, Ogawa M. 2004. Asymmetric production of surface-dividing and non-surface-dividing cortical progenitor cells. *Development*. 131:3133–3145.

Molnar Z, Kaas JH, de Carlos JA, Hevner RF, Lein E, Nemec P. 2014. Evolution and development of the mammalian cerebral cortex. *Brain Behav Evol*. 83:126–139.

Nelson B, Martínez-Cerdeño V, Cunningham CL, Camacho J, Antczak JL, Prakash AN, Cziep ME, Walker AI, Noctor SC. 2012. Comparative analysis of the subventricular zone in rat, ferret and macaque: evidence for an outer subventricular zone in rodents. *PLoS One*. 7:e30178.

Noctor SC, Martinez-Cerdeno V, Ivic L, Kriegstein AR. 2004. Cortical neurons arise in symmetric and asymmetric division zones and migrate through specific phases. *Nat Neurosci*. 7:136–144.

Rakic P. 2003. Developmental and evolutionary adaptations of cortical radial glia. *Cereb Cortex*. 13:541–549.

Rakic P. 2009. Evolution of the neocortex: a perspective from developmental biology. *Nat Rev Neurosci*. 10:724–735.

Rash BG, Duque A, Morozov YM, Arellano JI, Micali N, Rakic P. 2019. Gliogenesis in the outer subventricular zone promotes enlargement and gyrification of the primate cerebrum. *Proc Natl Acad Sci*. 116:7089–7094.

Reillo I, de Juan Romero C, Garcia-Cabezas MA, Borrell V. 2011. A role for intermediate radial glia in the tangential expansion of the mammalian cerebral cortex. *Cereb Cortex*. 21:1674–1694.

Romer S, Bender H, Knabe W, Zimmermann E, Rubsamen R, Seeger J, Fietz SA. 2018. Neural progenitors in the developing neocortex of the northern tree shrew (*Tupaia belangeri*) show a closer relationship to gyrencephalic primates than to lissencephalic rodents. *Front Neuroanat*. 12:29.

Sauerland C, Menzies BR, Glatzle M, Seeger J, Renfree MB, Fietz SA. 2018. The basal radial glia occurs in marsupials and underlies the evolution of an expanded neocortex in Therian mammals. *Cereb Cortex*. 28:145–157.

Shitamukai A, Konno D, Matsuzaki F. 2011. Oblique radial glial divisions in the developing mouse neocortex induce self-renewing progenitors outside the germinal zone that resemble primate outer subventricular zone progenitors. *J Neurosci*. 31:3683–3695.

Smart IH, Dehay C, Giroud P, Berland M, Kennedy H. 2002. Unique morphological features of the proliferative zones and postmitotic compartments of the neural epithelium giving rise to striate and extrastriate cortex in the monkey. *Cereb Cortex*. 12:37–53.

Taverna E, Gotz M, Huttner WB. 2014. The cell biology of neurogenesis: toward an understanding of the development and evolution of the neocortex. *Annu Rev Cell Dev Biol*. 30:465–502.

Tyler WA, Haydar TF. 2013. Multiplex genetic fate mapping reveals a novel route of neocortical neurogenesis, which is altered in the Ts65Dn mouse model of down syndrome. *J Neurosci*. 33:5106–5119.

Vasistha NA, Garcia-Moreno F, Arora S, Cheung AF, Arnold SJ, Robertson EJ, Molnar Z. 2015. Cortical and clonal contribution of Tbr2 expressing progenitors in the developing mouse brain. *Cereb Cortex*. 25:3290–3302.

Wang X, Tsai J-W, LaMonica B, Kriegstein AR. 2011. A new subtype of progenitor cell in the mouse embryonic neocortex. *Nat Neurosci*. 14:555–561.

Wong P, Kaas JH. 2009. Architectonic subdivisions of neocortex in the tree shrew (*Tupaia belangeri*). *Anat Rec (Hoboken)*. 292:994–1027.

Yan LZ, Sun B, Lyu LB, Ma YH, Chen JQ, Lin Q, Zheng P, Zhao XD. 2016. Early embryonic development and transplantation in tree shrews. *Dongwuxue Yanjiu*. 37:252–258.

Yao YG. 2017. Creating animal models, why not use the Chinese tree shrew (*Tupaia belangeri* chinensis)? *Zool Res*. 38:118–126.

Supplementary Figure 1

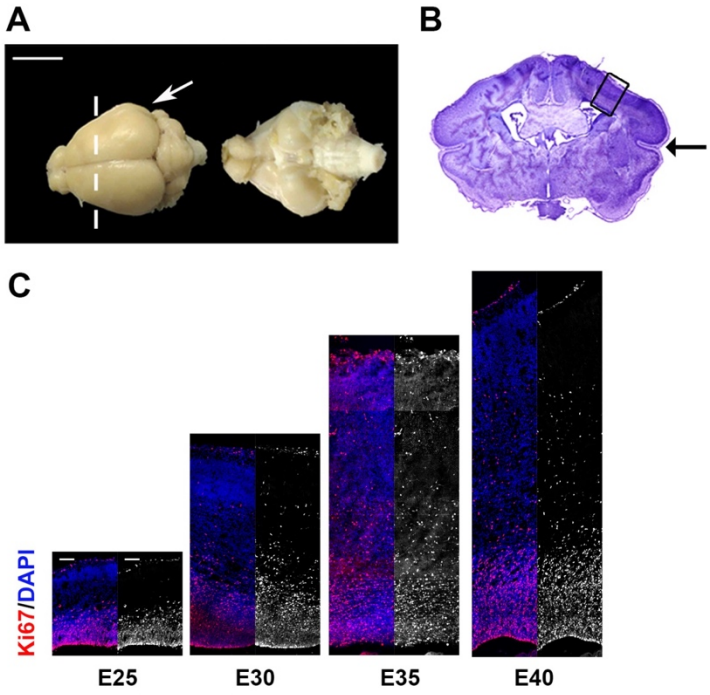

Figure S1. Compartmentalization of the Chinese tree shrew neocortex. (A) Front and bottom views of an adult tree shrew brain. The arrow indicates the major fissure, and the dotted line indicates location of the section used for Nissl staining; Scale bar: 1 cm.（B）Overview of a coronal section of the adult Chinese tree shrew forebrain. The arrows in A and B indicate the rhinal fissure. (C) Ki67 immunostaining revealing proliferative regions. At E25, the VZ and the SVZ were present. After E30, the SVZ was expanded and subdivided into the iSVZ and the oSVZ. Proliferation was still high at E40. Scale bars: 100 μm. VZ, ventricular zone; SVZ, subventricular zone; IZ, intermediate zone; CP, cortical plate; MZ, marginal zone; Scale bar: 100 μm.

Multiple comparison analysis

(Related to Figure 2E)

Tukey's multiple comparisons test	Significant?	Summary	Adjusted P Value
	$Sox2^+$ cells in the VZ		
E25 vs. E30	No	ns	0.9767
E25 vs. E35	No	ns	0.1286
E25 vs. E40	Yes	**	0.0068
E30 vs. E35	No	ns	0.2225
E30 vs. E40	Yes	*	0.0113
E35 vs. E40	No	ns	0.2134
	$Sox2^+$ cells in the iSVZ		
E25 vs. E30	Yes	**	0.0013
E25 vs. E35	Yes	****	<0.0001
E25 vs. E40	Yes	****	<0.0001
E30 vs. E35	Yes	****	<0.0001
E30 vs. E40	Yes	****	<0.0001
E35 vs. E40	No	ns	0.487
	$Sox2^+$ cells in the oSVZ		
E25 vs. E30	N/A	N/A	N/A
E25 vs. E35	N/A	N/A	N/A
E25 vs. E40	N/A	N/A	N/A
E30 vs. E35	Yes	****	<0.0001
E30 vs. E40	Yes	****	<0.0001
E35 vs. E40	No	ns	0.96

(Related to Figure 2F)

Tukey's multiple comparisons test	Significant?	Summary	Adjusted P Value
	Tbr2^{+} cells in the iSVZ		
E30 vs. E35	Yes	***	0.0007
E30 vs. E40	Yes	**	0.0013
E35 vs. E40	No	ns	0.7121
	Tbr2^{+} cells in the oSVZ		
E30 vs. E35	Yes	*	0.0491
E30 vs. E40	Yes	****	<0.0001
E35 vs. E40	Yes	****	<0.0001

(Related to Figure 2G)

Sidak's multiple comparisons test	Significant?	Summary	Adjusted P Value
	E30 iSVZ - E30 oSVZ		
$Sox2^+$ $Tbr2^+$	No	ns	0.335
$Sox2^-$ $Tbr2^+$	Yes	****	<0.0001
$Sox2^+$ $Tbr2^-$	Yes	****	<0.0001
	E35 iSVZ - E35 oSVZ		
$Sox2^+$ $Tbr2^+$	No	ns	0.9982
$Sox2^-$ $Tbr2^+$	No	ns	0.9353
$Sox2^+$ $Tbr2^-$	No	ns	0.8741
	E40 iSVZ - E40 oSVZ		
$Sox2^+$ $Tbr2^+$	Yes	*	0.0256
$Sox2^-$ $Tbr2^+$	Yes	***	0.0008
$Sox2^+$ $Tbr2^-$	No	ns	0.1993

(Related to Figure 4C)

Tukey's multiple comparisons test	Significant?	Summary	Adjusted P Value
	Percetaage of triple positive cells in the VZ		
E25 vs. E35	Yes	****	<0.0001
E25 vs. E40	Yes	****	<0.0001
E30 vs. E35	Yes	**	0.0091
E30 vs. E40	Yes	***	0.0003
E35 vs. E40	No	ns	0.0671
	Percetaage of triple positive cells in the iSVZ		
E25 vs. E30	No	ns	0.2336
E25 vs. E35	No	ns	0.701
E25 vs. E40	Yes	**	0.0012
E30 vs. E35	No	ns	0.7557
E30 vs. E40	Yes	*	0.0151
E35 vs. E40	Yes	**	0.0043
	Percetaage of triple positive cells in the oSVZ		
E25 vs. E30	N/A	N/A	N/A
E25 vs. E35	N/A	N/A	N/A
E25 vs. E40	N/A	N/A	N/A
E30 vs. E35	No	ns	0.2025
E30 vs. E40	Yes	***	0.0003
E35 vs. E40	Yes	***	0.001